Cell, Vol. 84, 37–47, January 12, 1996, Copyright ©1996 by Cell Press

XKCM1: A Xenopus Kinesin-Related Protein That Regulates Microtubule Dynamics during Mitotic Spindle Assembly

Claire E. Walczak,* Timothy J. Mitchison,* and Arshad Desai†
*Department of Cellular and Molecular Pharmacology
University of California, San Francisco
San Francisco, California 94143-0450
†Department of Biochemistry and Biophysic
University of California, San Francisco
San Francisco, California 94143-0448

Summary

We isolated a cDNA clone encoding a kinesin-related protein, which we named XKCM1. Antibodies to XKCM1 stain mitotic centromeres and spindle poles. Immunodepletion and antibody addition experiments in an in vitro spindle assembly assay show that XKCM1 is required for both establishment and maintenance of mitotic spindles. The structures that form in the absence of XKCM1 contain abnormally long microtubules. This long microtubule defect can be rescued by the addition of purified XKCM1 protein. Analysis of microtubule dynamics in a clarified mitotic extract reveals that loss of XKCM1 function causes a 4-fold suppression in the catastrophe frequency. XKCM1 thus exhibits a novel activity for a kinesin-related protein by promoting microtubule depolymerization during mitotic spindle assembly.

Introduction

The faithful segregation of genetic material to daughter cells is essential for the survival of an organism. This process is carried out by the mitotic spindle, which consists of a dynamic array of microtubules responsible for distributing replicated sister chromatids to each daughter cell.

Microtubules are polar polymers that exhibit nonequilibrium polymerization dynamics termed dynamic instability (Mitchison and Kirschner, 1984). Microtubules can coexist in both growing and shrinking states; these states interconvert frequently and stochastically both in vitro and in vivo. Dynamic instability is thought to provide microtubules with the ability to search three-dimensional space more effectively than would be possible for a simple equilibrium polymer (Holy and Leibler, 1994). Perhaps this ability evolved to allow the rapid capture of chromosomes by microtubules during the early stages of spindle assembly (reviewed by Kirschner and Mitchison, 1986). Consistent with this idea is the observation that microtubule turnover increases dramatically during mitosis relative to interphase (Salmon et al., 1984; Saxton et al., 1984). This increase in microtubule turnover probably plays a crucial role in the assembly of the mitotic spindle (reviewed by Inoué and Salmon, 1995).

Detailed analysis of the cell cycle regulation of microtubule behavior has been performed in Xenopus egg extracts (Belmont et al., 1990; Verde et al., 1990, 1992). These studies showed, first, that the polymerization dynamics of microtubules in vivo is significantly different from that of pure tubulin, suggesting the presence of cellular factors that regulate dynamics, and, second, that microtubules in mitosis are much more dynamic than those in interphase, primarily as a result of an increase in the frequency of transitions from the growth state to the shrinkage state (catastrophes), suggesting that there exist one or more cell cycle–regulated factors that affect microtubule dynamics. These phenomenological observations have yet to be extended to molecular mechanisms.

In addition to cell cycle–dependent regulation of bulk spindle microtubule dynamics, real-time analysis of the behavior of chromosomes in spindles suggests that chromosomes possess the ability to modulate the polymerization dynamics of a subset of spindle microtubules attached at their kinetochores. Extensive live analysis of cells undergoing mitosis has shown that chromosomes constantly oscillate on the mitotic spindle (Bajer, 1982; Skibbens et al., 1993). For a chromosome to change direction, the kinetochore must catalyze a coordinate switch in the polymerization state of its kinetochore microtubules.

In addition to regulating dynamics, kinetochores may couple the movement of chromosomes to the polymerization/depolymerization cycles of spindle microtubules to power chromosome movement (reviewed by Rieder and Salmon, 1994; Inoué and Salmon, 1995). Alternatively, mechanochemical motor proteins targeted to kinetochores may move chromosomes by translocating along spindle microtubules. Support for the latter hypothesis came from the localization of three motor proteins, cytoplasmic dynein and the kinesin-related proteins (KRPs) centromere protein E (CENP-E) and mitotic centromere-associated kinesin (MCAK), to mammalian kinetochores (Pfarr et al., 1990; Steuer et al., 1990; Yen et al., 1991; Wordeman and Mitchison, 1995). A recent in vitro study on CENP-E and kinesin has led to a unifying view of these two hypotheses by showing that motor molecules can couple their attached cargo to depolymerizing microtubules (Lombillo et al., 1995a, 1995b). These studies suggest that, in addition to moving along spindle microtubules, motor proteins at the kinetochore may be able to couple the movement of chromosomes directly to depolymerizing spindle microtubules (reviewed by Desai and Mitchison, 1995). Although these findings hint at how a chromosome can move along a depolymerizing microtubule, they leave open the question of how chromosomes switch their direction of movement on the spindle as they oscillate.

To explore further the mechanisms of mitotic spindle assembly and chromosome dynamics, we isolated KRPs from Xenopus that might be important in these processes. Xenopus egg extracts provide both a manipulable in vitro system to examine motor function during spindle assembly and a biochemically enriched source of material required for mitosis. We used an antibody to a conserved region of the kinesin motor domain

(Sawin et al., 1992b) to isolate clones encoding KRPs from a Xenopus ovary cDNA library. One of the identified KRPs, which we named XKCM1 (for Xenopus kinesin central motor 1), is essential for mitotic spindle assembly in vitro, localizes to centromeres, and appears to regulate the polymerization dynamics of microtubules, a novel activity for a KRP.

Results

Identification and Characterization of XKCM1

To identify KRPs important for mitotic spindle assembly and function, we screened a Xenopus ovary cDNA library with the anti-HIPYR peptide antibody, which was raised against a conserved sequence in kinesin motor domains (Sawin et al., 1992b). The most abundant clone isolated (56 of 75) encoded the protein XKCM1. Other clones isolated in this screen will be described elsewhere.

The cDNA for XKCM1 is 2402 nt in length and encodes a 730 amino acid protein with a predicted molecular mass of 83 kDa (Figure 1A). Based on high sequence homology, XKCM1 belongs to the KIF2 family of kinesins, originally identified in a screen for KRPs important in neuronal vesicular transport (Aizawa et al., 1992). The closest homolog of XKCM1 is MCAK, which was isolated from CHO cells in a screen similar to the one described here (Wordeman and Mitchison, 1995).

Structural analysis of the XKCM1 sequence predicts a protein with a 250 amino acid amino-terminal globular domain, a centrally located 350 amino acid motor domain, and a 130 amino acid α-helical tail, portions of which are predicted to form an α-helical coiled coil (Lupas et al., 1991) (Figure 1B). To generate reagents to probe the function of XKCM1, we raised polyclonal antibodies to a glutathione S-transferase fusion protein containing the amino-terminal globular domain of XKCM1. These affinity-purified antibodies recognized a doublet in Xenopus egg extracts with a molecular mass of 85 kDa, close to the predicted size of the XKCM1 protein (Figure 1C, lanes 1 and 2). We estimate that XKCM1 is present at approximately 10 μg/ml in these extracts. In addition, these antibodies were able to immunoprecipitate an 85 kDa doublet from Xenopus egg extracts (Figure 3A).

To show that XKCM1 has properties consistent with it being a KRP, we performed microtubule binding experiments (Figure 1C). Xenopus egg high speed supernatants were incubated in the presence of AMP-PNP, taxol, and an ATP depletion system. The assembled microtubules were sedimented along with bound proteins, and the release of XKCM1 from microtubules was analyzed using different extraction conditions. XKCM1 quantitatively sedimented with microtubules under ATP depletion conditions (Figure 1C, lanes 1 and 2). In addition, XKCM1 was released from microtubules with a combination of ATP and 0.5 M NaCl (Figure 1C, lanes 9 and 10), but was not released from microtubules with either ATP or 0.5 M NaCl (lanes 3–6).

XKCM1 Is Found on Centromeres and Centrosomes during Mitosis

We determined the localization of XKCM1 in both tissue culture cells and mitotic spindles assembled in vitro. In the Xenopus tissue culture cell line, XL177, the immunolocalization of XKCM1 was quite complex. During interphase, the protein was found as a soluble pool present in both the nucleus and the cytoplasm (Figure 2A, I); this soluble pool persisted throughout mitosis, but was most apparent during prometaphase to telophase, when the cells are most rounded. In addition, a portion of XKCM1 localized during mitosis to the centromeric region of the mitotic chromosomes and to the centrosomal region of the spindle (Figure 2A, PM to T). Centromeric localization persisted throughout mitosis and decreased in intensity by anaphase, but could still be detected at telophase (Figure 2A, A and T). Localization to the centrosomal region of the spindle was evident from prometaphase to anaphase (Figure 2A, PM to A).

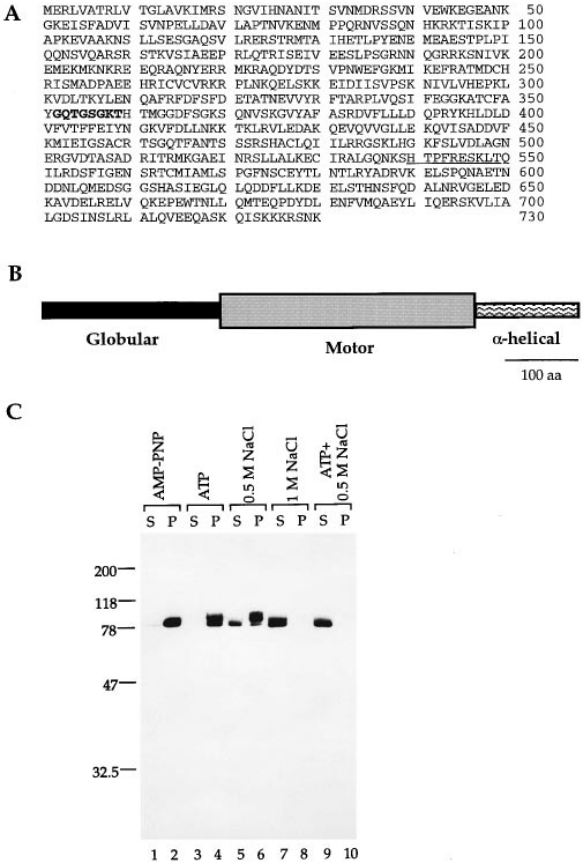

Figure 1. XKCM1 Is a KRP

(A) The deduced amino acid sequence of XKCM1. The putative P loop is indicated in bold, and the conserved peptide sequence recognized by the anti-HIPYR peptide antibody used to isolate the clone is underlined.

(B) A schematic representation of XKCM1 structure. XKCM1 contains an amino-terminal globular domain, a central motor domain, and a carboxy-terminal α-helical tail.

(C) Immunoblots of microtubule pelleting assays in Xenopus egg extracts. Microtubules were polymerized in mitotic high speed supernatants of Xenopus egg extracts and pelleted in the absence of ATP and the presence of AMP-PNP (lanes 1 and 2). The microtubule pellet, with associated proteins, was resuspended and extracted with 2 mM Mg–ATP (lanes 3 and 4), 0.5 M NaCl (lanes 5 and 6), 1 M NaCl (lanes 7 and 8), or 2 mM Mg–ATP plus 0.5 M NaCl (lanes 9 and 10). The blots were probed with anti-XKCM1.

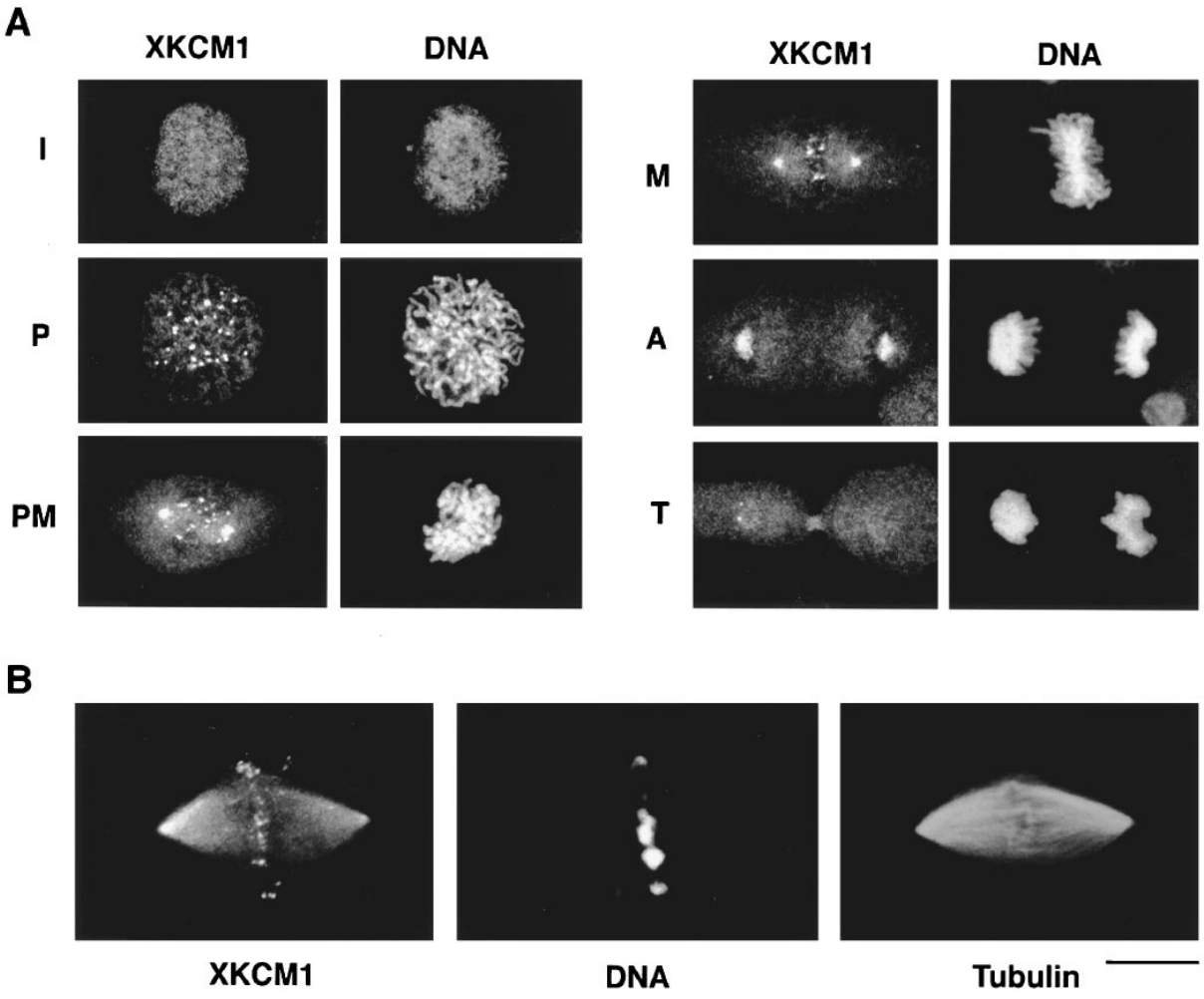

Figure 2. Immunolocalization of XKCM1

(A) Immunolocalization of XKCM1 in Xenopus tissue culture cells. The cells were stained with 1 μg/ml anti-XKCM1 followed by fluorescein isothiocyanate (FITC)-conjugated goat anti-rabbit secondary antibody. DNA was visualized by staining with 0.05 μg/ml propidium iodide. Images were recorded on a Bio-Rad MRC-600 laser scanning confocal microscope. Interphase (I), prophase (P), prometaphase (PM), metaphase (M), anaphase (A), and telophase (T) are shown. Scale bar is 20 μm.

(B) Immunolocalization of XKCM1 on in vitro assembled spindles. Mitotic spindles assembled in vitro were isolated onto coverslips, fixed, and stained with anti-XKCM1, followed by FITC-conjugated goat anti-rabbit secondary antibody. DNA was visualized by staining with Hoechst 33528, and microtubules were visualized by adding rhodamine tubulin to extracts. Images were recorded with a Zeiss Photomicroscope III. Scale bar is 20 μm.

This localization is consistent with the immunolocalization and biochemical analysis of MCAK, the CHO cell homolog of XKCM1 (Wordeman and Mitchison, 1995). The observed localization was competed by inclusion of the amino-terminal fusion protein in the primary antibody solution and was not observed with a nonimmune immunoglobulin G (IgG) antibody or with antibodies to two other Xenopus KRPs, indicating that the staining is specific for the XKCM1 antibodies (data not shown). If cells were permeabilized before antibody staining, XKCM1 was found all along microtubules in both mitotic and interphase cells. This staining was eliminated by inclusion of ATP in the permeabilization buffer, suggesting that it is the result of ATP depletion during permeabilization and subsequent rigor binding of the motor to microtubules (data not shown).

On spindles assembled in vitro, XKCM1 was found at the centromeric regions as well as at the centrosomes, but there was also a diffuse staining of the entire spindle (Figure 2B). This more diffuse staining along the length of spindle microtubules could not be reduced by increasing the ATP concentration during the isolation procedure, suggesting that it may represent a true difference in XKCM1 distribution between in vitro assembled spindles and those in tissue culture cells. Another possibility is that there are more microtubules in in vitro assembled spindles, and we thus see a higher intensity of staining.

XKCM1 Is Required for Assembly and Maintenance of the Mitotic Spindle

To probe the function of XKCM1, we took advantage of the ability to form mitotic spindles in vitro in Xenopus egg extracts. Upon addition of sperm chromatin to a

mitotically arrested Xenopus egg extract, there is a time-dependent formation of a mitotic spindle (Lohka and Maller, 1985; Sawin and Mitchison, 1991; Shamu and Murray, 1992). We investigated the effect of XKCM1 removal on this process. We estimate that greater than 99% of XKCM1 could be removed from the extract by immunodepletion, with a quantitative recovery of the protein in the immunoprecipitated pellet (Figures 3A and 3B, lanes 1 and 2). In mock-depleted extracts (using generic rabbit IgG as a control), there was a time-dependent formation of a bipolar spindle (Figures 4A and 4B). Over 70% of the nuclei formed a classic spindle-like structure (Figure 5A). When XKCM1 was removed from the extract, there was a gross morphological disruption of mitotic spindle assembly. At early timepoints, abnormally large microtubule asters formed, which had centrally located chromatin with microtubules emanating in a sunburst pattern from the center of the structure (Figure 4C). With time, the XKCM1-depleted extracts formed huge aggregated structures with long microtubules radiating from the outer portion of the structure (Figure 4D). Over 90% of added nuclei participated in forming distorted structures in the XKCM1-depleted extracts (Figure 5A). The same results were obtained if antibodies to XKCM1 were added to extracts prior to spindle assembly (data not shown). A final concentration of antibody in the extract as low as 10 μg/ml resulted in the same aberrant structures as in the immunodepleted extracts. Although the long microtubules seen in the XKCM1-immunodepleted extract are reminiscent of interphase-length microtubules, the extract remained mitotic, as indicated by the condensed chromatin and high levels of histone H1 kinase activity (data not shown). When antibodies to XKCM1 were added to extracts that had already formed spindles, there was a rapid perturbation of spindle structure (< 2 min) beginning with growth of long microtubules from the outer parts of the spindle and eventually resulting in huge, distorted structures that were indistinguishable from those induced by antibody addition prior to spindle assembly or by immunodepletion (data not shown). Taken together, these results show that XKCM1 is required both for assembly and maintenance of normal spindle structure in vitro.

The endogenous level of XKCM1 is important for spindle assembly. We found that removing as little as 25% of the XKCM1 from extracts resulted in aberrant structures with morphology similar to those in the fully depleted extract. This suggests that the concentration of XKCM1 present in the extract is important for proper spindle assembly (data not shown).

Isolated XKCM1 Rescues the Defect in Depleted Extracts

To prove that the observed disruption of spindle assembly is specifically due to XKCM1 removal, we purified the native protein from Xenopus egg extracts to add back to depleted extracts. We synthesized a peptide to the carboxy-terminal ten amino acids of XKCM1 (XKCM1-CTP) and used this peptide for the production of polyclonal antibodies. These antibodies were able to immunodeplete XKCM1 from extracts and caused the same spindle assembly defects seen using the anti-XKCM1 antibodies raised to the entire amino-terminal domain of XKCM1 (data not shown). We used these peptide antibodies to purify XKCM1 by immunoaffinity chromatography. Ammonium sulfate cuts of Xenopus egg high speed supernatants were passed over a column of XKCM1-CTP antibodies immobilized on protein A resin. The flowthrough fraction of the column contained the majority of the total extract protein (Figure 3C, lanes L and F). The bound protein on the column was eluted with XKCM1-CTP peptide (Figure 3C, lanes 1–10). Fractions 2–6 of the XKCM1 eluted from the affinity column were pooled, concentrated, and used for reconstitution of spindle assembly. We estimate that the protein is on average 90% pure using this procedure.

We immunodepleted XKCM1 from Xenopus egg extracts and then added back purified XKCM1 prior to spindle assembly to determine whether the pure protein could rescue the defect in the depleted extracts. The amount of XKCM1 added back to the immunodepleted extract was equivalent to the amount present endogenously in extracts as judged by quantitative blotting (Figure 3B, lane 3). Addition of purified XKCM1 suppressed the long microtubule phenotype, proving that

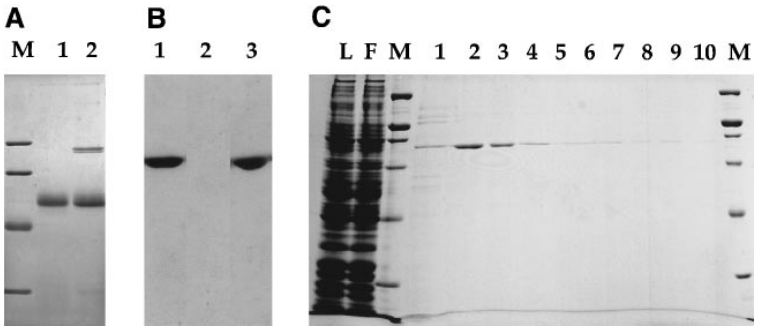

Figure 3. Biochemical Analysis of XKCM1 Protein

(A) Immunoprecipitation of XKCM1 from egg extracts. Immunoprecipitation was performed using control rabbit IgG (lane 1) or affinity-purified anti-XKCM1 (lane 2). The protein A complexes were washed, separated by 10% SDS–PAGE, and visualized by staining with Coomassie blue. Molecular mass markers (M) are 97, 66, 45, and 31 kDa.

(B) Immunodepletion and addback of XKCM1 to extracts. CSF extracts were immunodepleted with control IgG (lane 1), anti-XKCM1 (lane 2), or anti-XKCM1, followed by the addition of purified XKCM1 protein (lane 3). The extracts were separated by 10% SDS–PAGE, transferred to nitrocellulose, and then probed with anti-XKCM1.

(C) Affinity purification of XKCM1. XKCM1 was purified on an affinity column of anti-peptide antibodies that recognize the carboxyl terminus of XKCM1. Fractions were eluted with XKCM1 carboxy-terminal peptide, precipitated with trichloroacetic acid, separated by 10% SDS–PAGE, and visualized by staining with Coomassie. The column load (L) was a 25%–40% ammonium sulfate cut of a Xenopus egg extract. Also shown are the flowthrough of column (F) and fractions 1–10 (1 column volume each). Molecular mass markers (M) are 200, 116, 97, 66, 45, and 31 kDa. Fractions 2–6 were pooled, concentrated, and used in the functional reconstitution.

the observed defect is mediated by loss of XKCM1 (Figure 4E). We did not observe a high percentage of bipolar mitotic spindles in the rescued extracts, but this was also true for a mock-depleted extract with control buffer added back. Thus, the reconstituted structures (Figure 4E) resembled those in a control extract that had undergone the same series of manipulations (data not shown). The reconstituted spindles were often less fusiform shaped and smaller and had a less organized microtubular array compared with spindles that assembled in an unperturbed extract. Pure XKCM1 must be added back to extracts at a concentration similar to that found endogenously in extracts in order for it to rescue the depleted extracts. If too little XKCM1 was added back to the immunodepleted extract, we were unable to suppress the long microtubule phenotype. In combination with partial immunodepletion experiments (see above), this strongly suggests that the concentration of XKCM1 in extracts is critical for proper spindle assembly. To quantitate the reconstitution, we measured the area of control spindles, XKCM1-depleted structures, and reconstituted structures (Figure 5B). XKCM1-immunodepleted structures were approximately ten times larger than mock-depleted structures. This means that the longest microtubules were increased in length an average of 10-fold, although their high density precluded accurate length measurements. Addition of purified XKCM1 to the immunodepleted extract resulted in structures that were the same size as controls. These results strongly suggest that loss of XKCM1 function by removal of the protein from extracts is responsible for the observed long microtubules.

Loss of XKCM1 Function Alters Microtubule Dynamics

The extremely long microtubules seen in the XKCM1-depleted structures suggested that some aspect of microtubule dynamics might be altered in the absence of XKCM1 function. To test this possibility, we measured the parameters of microtubule dynamic instability in high

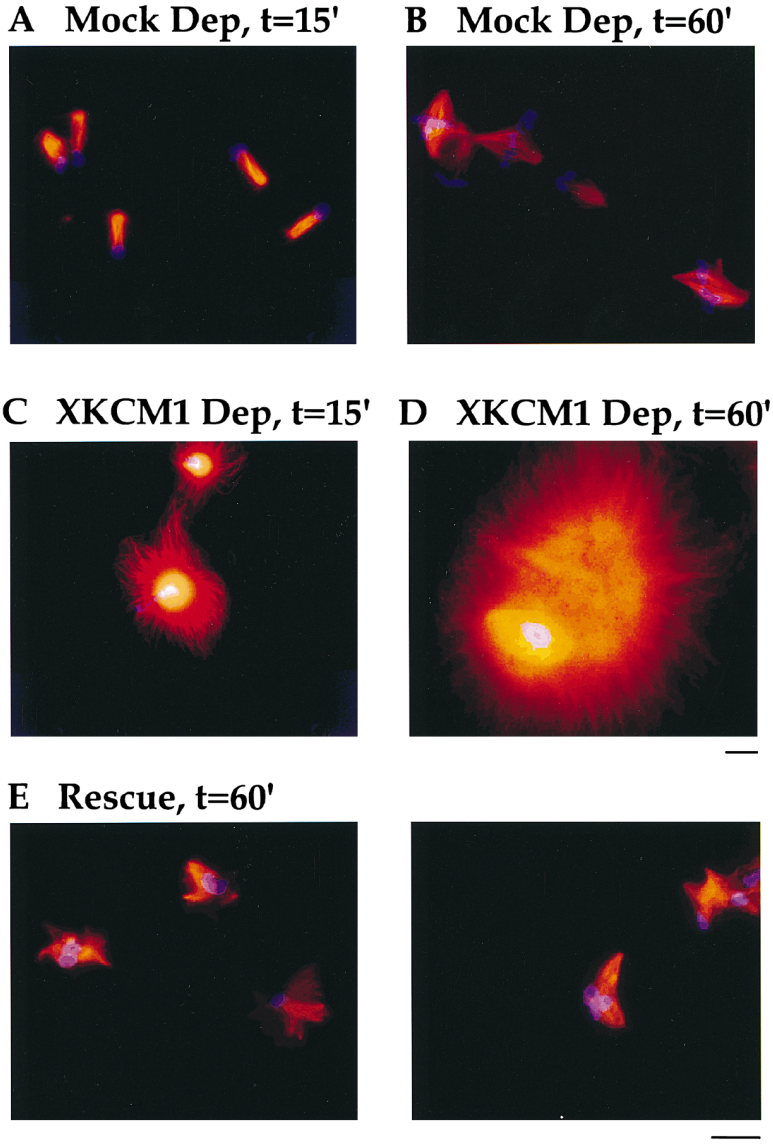

Figure 4. XKCM1 Is Required for Mitotic Spindle Assembly

Mitotic spindles were assembled in a mock-depleted extract (A and B) or an XKCM1-depleted extract (C and D). Two timepoints are shown for each assembly condition. In the absence of XKCM1, huge microtubule asters form. The bright white spot in the center of the aster is where the DNA (blue) and tubulin (red) are overlayed and have saturated the film. Scale bar for (A)–(D) is 20 μm.

(E) Mitotic spindles were assembled in XKCM1-immunodepleted extracts that were reconstituted by the addition of purified XKCM1 prior to spindle assembly. The long microtubules seen in the immunodepleted extracts are no longer present; instead, structures resembling mitotic spindles are formed. Two representative fields of view are shown. Rhodamine-labeled microtubules are shown in red, and DNA is in blue. Scale bar is 20 μm.

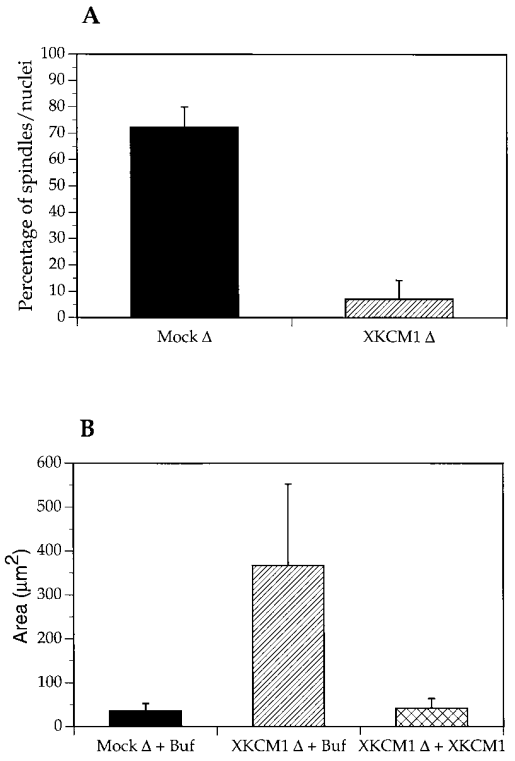

Figure 5. Quantitation of XKCM1 Immunodepletion and Rescue with Pure XKCM1

(A) Effect of XKCM1 immunodepletion on spindle assembly. Mitotic spindles were assembled in either mock-depleted extracts (Mock Δ) or in XKCM1-depleted extracts (XKCM1 Δ). Structures that assembled were sedimented onto coverslips, and the percentage of spindle-like structures that formed per nuclei was quantitated. The bars represent mean ± 95% confidence interval of ten independent experiments (n = 2927 nuclei for mock-depleted samples; n = 2961 nuclei for XKCM1-depleted samples).

(B) Reconstitution of spindle assembly with purified XKCM1. Mitotic spindles were assembled in mock-depleted extracts with control buffer added (Mock Δ plus Buf), in XKCM1-depleted extracts with control buffer added (XKCM1 Δ plus Buf), or in XKCM1-depleted extracts that were reconstituted by the addition of purified XKCM1 (XKCM1 Δ plus XKCM1). Structures were sedimented onto coverslips, and the area was measured as described in Experimental Procedures. The bars represent the mean area ± 1 SD for the area of 100 structures measured in each condition in a single experiment, but are representative of data from three separate experiments.

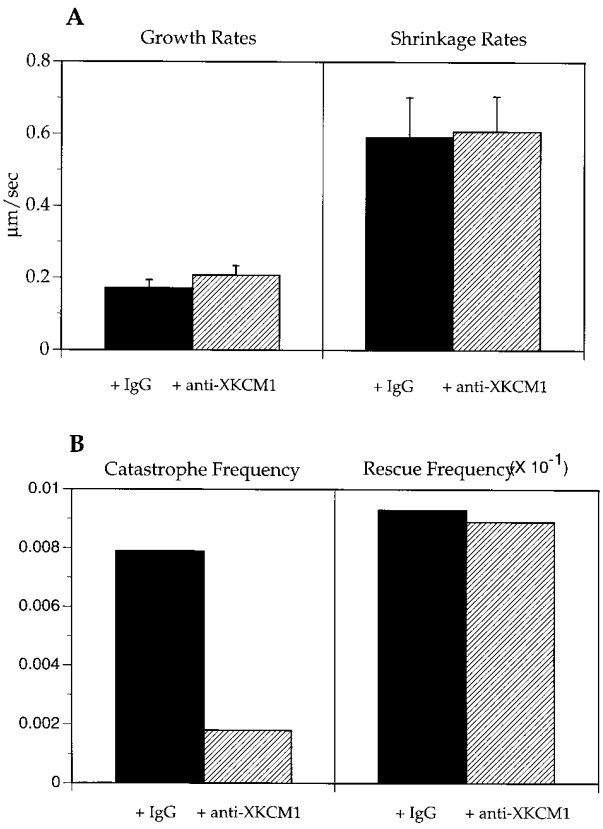

Figure 6. Removal of XKCM1 Suppresses Catastrophes in Mitotic High Speed Supernatants

We measured the parameters of microtubule dynamics in extracts that had either control IgG or XKCM1 antibodies added. There was no significant difference in the growth or shrinkage rates (A) with either antibody addition (n = 34 microtubules for IgG addition; n = 60 microtubules for anti-XKCM1 addition). There was, however, a 4-fold suppression of the catastrophe frequency (B) in the presence of XKCM1 antibodies (t_{growth} = 2922 s for IgG addition; t_{growth} = 6167 s for anti-XKCM1 addition). There was no significant difference in the rescue frequency (B) with either antibody addition (t_{shrink} = 215 s for IgG addition; t_{shrink} = 112 s for anti-XKCM1 addition), although it is difficult to measure accurately the rescue frequency in the absence of many catastrophes. The parameters were essentially identical for immunodepleted extracts.

speed supernatants of mitotic egg extracts in the presence of either control IgG or anti-XKCM1. We compared the growth rates and shrinkage rates, as well as the frequency of transitions from growth to shrinkage (catastrophe frequency) and the frequency of transitions from shrinkage to growth (rescue frequency). We found no significant difference in the growth rates or the shrinkage rates (Figure 6A). However, we found a 4-fold suppression in the catastrophe frequency in extracts that had anti-XKCM1 added relative to extracts that had control IgG added (Figure 6B). The rescue frequency did not differ significantly between the two conditions, although it was difficult to measure rescue accurately in the antibody-treated extracts owing to the limited number of observed catastrophes. We repeated our analysis of dynamics parameters on extracts that had been immunodepleted of XKCM1 and found that the measured parameters were essentially identical to those determined in the XKCM1 antibody addition experiments (data not shown). These results imply that XKCM1 acts as a catastrophe promoter in extracts. The loss of XKCM1 function causes a suppression of catastrophes, which results in the observed long microtubules.

Discussion

The KIF2 Family of Kinesins

XKCM1 belongs to a family of kinesins that contain centrally located motor domains. The parental member of this family, KIF2, was originally identified in mouse brain in a polymerase chain reaction (PCR) screen for motors important in neuronal vesicle transport (Aizawa et al., 1992). Subsequent reports have shown that mouse KIF2 is a fast (0.5 μm/s), plus end–directed microtubule motor

that associates with a subclass of neuronal vesicles. XKCM1 is 76% identical to KIF2 within the motor domain (and 48% identical overall). XKCM1 is also highly homologous to MCAK (79% identical in the motor domain and 55% identical overall), which was identified in CHO cells in a screen similar to that described here (Wordeman and Mitchison, 1995).

There are at least two and possibly three functionally distinct classes of motors within the KIF2 family. Phylogenetic analysis generates three subgroupings within the KIF2 family. XKCM1 groups with MCAK and rKRP2, a kinesin-related protein isolated from rat testes (Sperry and Zhao, submitted). XKCM1 and MCAK exhibit a similar pattern of localization in tissue culture cells, and an anti-MCAK monoclonal antibody cross-reacts with a 90 kDa polypeptide in Xenopus egg extracts (Wordeman and Mitchison, 1995). rKRP2 is expressed highly in testes and may function as a meiotic motor; its localization in tissue culture cells has yet to be determined. The second subclass of the KIF2 family contains KIF2 itself as well as a second Xenopus KIF2 homolog, which we isolated in our screen (C. E. W. and T. J. M., unpublished data). This partial clone, which we refer to as *XKIF2*, encodes a protein that is 96% identical to the motor domain of mouse KIF2 and 90% identical overall. The extent of sequence identity suggests that XKIF2 is likely to be the true functional homolog of mouse KIF2. The fact that there are two KIF2 homologs in Xenopus suggests that there may be two KIF2 homologs in other organisms as well, but they have yet to be identified. A third subgrouping within the KIF2 family contains a sole member, DSK1, which localizes to diatom spindle midzones and is important for spindle elongation (Wein and Cande, personal communication). DSK1 is only 26% identical overall, and 44% identical within the motor domain, to XKCM1. It is unclear whether the lower homology and the functional differences between DSK1 and other KIF2 family members are a result of evolutionary divergence or if there is a third KIF2 subclass in all organisms.

Biochemical Properties of XKCM1

XKCM1 has properties consistent with it being a microtubule motor protein. In extracts, the protein binds and releases from microtubules in an ATP-dependent manner. Although we have not yet been able to demonstrate motor activity using either purified preparations of XKCM1 or a bacterially expressed version of XKCM1 in an in vitro microtubule gliding assay, we believe that XKCM1 will likely be a plus end–directed microtubule motor, given the high sequence identity with KIF2 within the motor domain.

Preliminary analysis of the behavior of XKCM1 on both gel filtration and sucrose gradients suggests that XKCM1 exists as a dimer in extracts (C. E. W. and T. J. M., unpublished data). Based on our immunoprecipitation data, which showed no coprecipitation of any other proteins with XKCM1, and the purification of XKCM1, which also showed no associated proteins, we propose that XKCM1 functions as a simple dimer with no light chains. This does not rule out the possibility that XKCM1 interacts transiently with other proteins to carry out its function.

XKCM1 Regulates Microtubule Dynamics

XKCM1 appears to regulate the catastrophe frequency of microtubules in mitotic Xenopus egg extracts. It is unclear whether this is likely to be a general property of motor molecules or specific to this particular motor. For example, depletion of Eg5 or Xklp1, two mitotic KRPs, from Xenopus egg extracts does not distort the spindle as dramatically as XKCM1 immunodepletion (Sawin et al., 1992a; Vernos et al., 1995), suggesting that the control of microtubule dynamics by a motor protein is a specialized property of XKCM1. The minus end–directed kinesin Kar3 can depolymerize the minus ends of taxol-stabilized microtubules as it translocates along them, suggesting that this motor may also destabilize microtubules (Endow et al., 1994). However, it is unclear what relevance this has to the in vivo function of Kar3.

We have drawn a model (Figure 7A) depicting how XKCM1 might cause catastrophes of microtubules. XKCM1 is shown walking along microtubules toward the plus end. When it reaches the end of the microtubule, it causes a destabilization of the microtubule end, initiating catastrophic depolymerization of the microtubule. It has been shown that the end of a depolymerizing microtubule is frayed (Mandelkow et al., 1991; Chrétien et al., 1995). A motor at the end of a microtubule might tweak the protofilaments of the microtubule apart, thus triggering depolymerization. It has been shown more recently that KRPs cause a conformational change of tubulin upon binding (Hirose et al., 1995; Hoenger et al., 1995; Kikkawa et al., 1995). One could imagine that certain types of KRPs might cause different changes in the conformation of the end of the microtubule. Some KRPs, like XKCM1, could trigger a catastrophe, while other motors might have no effect or could even stabilize microtubule ends. In support of our model, we have preliminary evidence suggesting that purified XKCM1 destabilizes microtubules assembled in vitro. We are currently investigating in detail the mechanism by which pure XKCM1 affects the polymerization dynamics of pure tubulin.

XKCM1 Is Required for Spindle Assembly

Removal of XKCM1 function increases microtubule stability and thus blocks spindle assembly at an early stage. The fact that the XKCM1-depleted structures cannot reorganize and form an abnormally large spindle suggests that microtubule dynamics are indeed necessary for spindle formation.

One possible model of XKCM1 function is that it modulates the dynamics of microtubules between interphase and mitosis. It has been shown that during this cell cycle progression there is an increase in the microtubule catastrophe frequency in Xenopus egg extracts (Belmont et al., 1990). It is possible that XKCM1 is the catastrophe factor responsible for the difference between interphase and mitotic microtubule dynamics, but at the present time we have no evidence to support this model. Although a more careful analysis will be

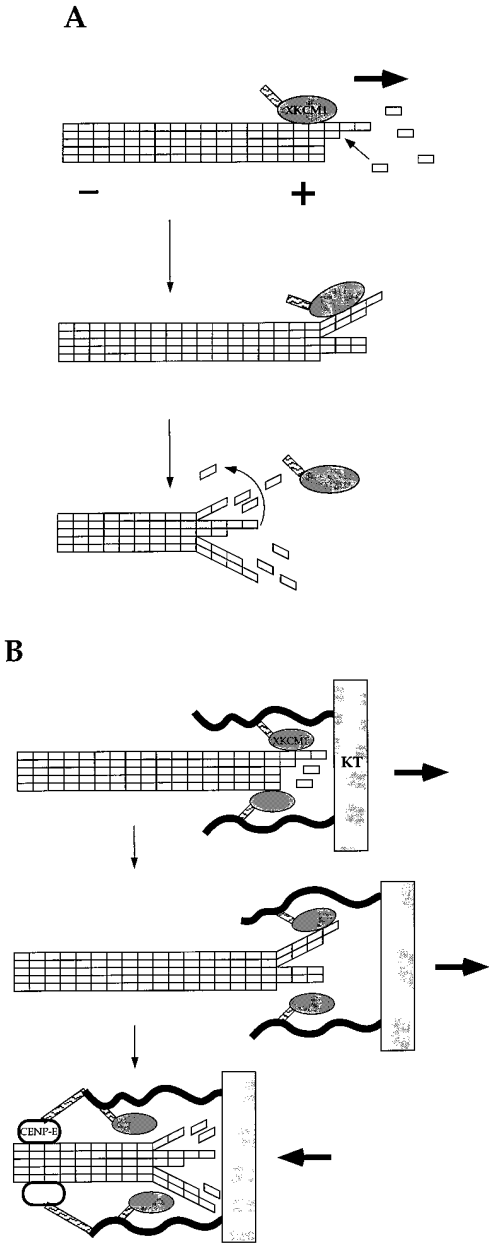

Figure 7. Model for XKCM1 Destabilization of Microtubules

(A) XKCM1 destabilizes microtubule ends. XKCM1 (stippled structure) walks along microtubules toward the plus end of a growing microtubule (indicated by subunit addition). As it approaches the end of the microtubule, it destabilizes the microtubule end, which results in microtubule depolymerization (indicated by subunit loss). XKCM1 is now free to bind to another microtubule and cause the same phenomenon.

(B) XKCM1 function at the kinetochore. XKCM1, bound to the kinetochore, walks along the microtubule, resulting in movement away from the pole. Upon reaching the end of the microtubule, it triggers a catastrophe resulting in depolymerization and movement back toward the pole. It is postulated that CENP-E acts to couple chromosome movement to the depolymerizing microtubule. (See text for further discussion).

necessary before making a judgment on this role, preliminary experiments looking at the effect of XKCM1 antibody addition to interphase extracts have also shown an increase in the number of microtubules present, suggesting that XKCM1 depolymerizing activity is active during interphase. We plan to explore the regulation of XKCM1 more thoroughly.

XKCM1 Function on Kinetochores

We favor a model that implicates XKCM1 function in the regulation of microtubule dynamics at the kinetochore (Figure 7B) in addition to its role in spindle assembly. An elegant high resolution video analysis of chromosome movement in Newt lung cells has shown that kinetochores oscillate throughout mitosis (Skibbens et al., 1993). It is thought that these oscillations are the result of switching between phases of growth and shrinkage of kinetochore microtubules. Microtubule motor proteins are attractive candidates for forming the transient linkage between a kinetochore and a microtubule because they are able to stay connected to a microtubule as they translocate along it. XKCM1 might act to regulate the transitions at the end of kinetochore microtubules. By being bound to the kinetochore, as demonstrated in our immunofluorescent staining, XKCM1 would be positioned near the end of the microtubule. It could then walk along a microtubule toward the plus end, possibly representing the plus end–directed kinetochore motor detected in vitro (Hyman and Mitchison, 1991). Upon reaching the end of the microtubule, XKCM1 would trigger a catastrophe. The chromosome would then move back toward the pole concomitant with microtubule depolymerization. It has been proposed that CENP-E might act as a kinetochore coupler to depolymerizing microtubules (Lombillo et al., 1995b; reviewed by Desai and Mitchison, 1995).

Earlier work by Hyman and Mitchison (1990) showed that isolated chromosomes could modulate the dynamics of microtubules in vitro, specifically that kinetochores increase the catastrophe rate of their bound microtubules. This activity was inhibited in the presence of AMP-PNP, suggesting the need for a kinetochore ATPase to cause catastrophes. Perhaps XKCM1 represents the ATP-dependent kinetochore-bound catastrophe factor they saw in their assays. We plan to repeat the in vitro kinetochore depolymerization assays in the presence of our XKCM1-blocking antibody to address this putative role of XKCM1.

In summary, we have isolated a KRP that plays a unique role in mitotic spindle morphogenesis. XKCM1 appears to act by regulating microtubule dynamics. This activity is a novel activity for a KRP and, furthermore, represents the identification of a physiological regulator of catastrophes. Our experiments suggest that XKCM1 acts directly on microtubules, causing a destabilization and eventual depolymerization of the microtubule. To analyze the mechanism of this destabilization, it will be necessary to show definitively that purified XKCM1 increases the catastrophe frequency of pure microtubules in the absence of any other proteins that could also influence microtubule dynamics.

Experimental Procedures

Isolation of *XKCM1* Clone

Affinity-purified anti-HIPYR peptide antibody (Sawin et al., 1992b) was used to screen a λUni-ZAP Xenopus ovary cDNA library (Stratagene) according to standard procedures (Sambrook et al., 1989).

In brief, after plaque lifts, the filters were washed in TBST (20 mM Tris [pH 7.4], 150 mM NaCl, 0.1% Tween 20) and then incubated in boiling water for 5 min to reduce background (Kellogg and Alberts, 1992). The filters were washed in TBST and blocked overnight in TBST plus 5% nonfat dry milk plus 0.1% NaN_3. The primary antibody was diluted to 1 μg/ml in blocking buffer and incubated for 1.5 hr, followed by alkaline phosphatase–labeled goat anti-rabbit secondary antibody (Promega). Positive clones were detected using colorometric detection. We screened 900,000 plaques and isolated 75 positive clones. Plasmid DNA was obtained from each clone by in vivo excision according to the protocol of the manufacturer. HIPYR-positive clones were categorized by restriction mapping, PCR, Southern blotting, and sequencing. By these characterizations, we found that 56 of 75 clones encoded XKCM1. The other clones will be described elsewhere. A single cDNA clone, clone *11B*, was fully sequenced on both strands using Sequenase Version 2.0 (United States Biochemicals). Gaps and ambiguities were resolved using an automated DNA sequencer (performed by the Biomolecular Resource Center DNA Sequencing Facility at the University of California, San Francisco).

Protein Expression and Antibody Production

The region corresponding to amino acids 2–264 was inserted using PCR into pGEX-2T (Smith et al., 1988) (clone pGEX-11BNT) and into pMAL-CRI (clone pMAL-11BNT). The glutathione S-transferase fusion protein was used for rabbit antibody production (Berkeley Antibody), and the antibodies were affinity purified on the MBP fusion protein. Antibodies were affinity purified according to published procedures (Harlow and Lane, 1988). Antibodies (anti-XKCM1) were eluted from the affinity column with 100 mM glycine (pH 2.5), 150 mM NaCl, neutralized, and then dialyzed against 10 mM HEPES, (pH 7.2), 100 mM KCl before being concentrated for use in the experiments described.

A carboxy-terminal peptide antibody (anti-XKCM1-CTP) was generated against the synthetic peptide (C)QISKKKRSNK (synthesized by the Biomolecular Resource Center), which corresponds to the last ten amino acids of XKCM1. An amino-terminal cysteine was added to the peptide for sulfhydryl coupling. All peptide conjugation procedures and antibody affinity purification were as described previously (Sawin et al., 1992b). Antibodies were dialyzed and concentrated as described above.

Microtubule Pelleting Assays and Immunoblotting

High speed supernatants of Xenopus egg extracts were prepared from crude cytostatic factor (CSF)-arrested extracts (Murray, 1991) as described previously (Hirano and Mitchison, 1993). Extracts were thawed, diluted 2-fold with CSF–XB (10 mM K–HEPES [pH 7.7], 50 mM sucrose, 2 mM $MgCl_2$, 0.1 mM $CaCl_2$, 100 mM KCl, 5 mM EGTA), and centrifuged at 50,000 rpm for 15 min in a TLA 100 rotor (Beckman). An ATP depletion system (15 U/ml hexokinase, 20 U/ml apyrase, 20 mM glucose) was added, as well as 10 μM taxol and 2 mM Mg–AMP-PNP. The extract was incubated for 30 min at 25°C and then layered onto a 1 ml cushion of 40% glycerol in Na–BRB80 (80 mM Na–PIPES [pH 6.8], 1 mM $MgCl_2$, 1 mM EGTA) and centrifuged in a TLA 100.3 rotor for 20 min at 60,000 rpm and 25°C. An aliquot was removed from the top of the cushion and saved for gel and immunoblot analysis. The pellets were washed and resuspended in BRB80 plus 10 μM taxol plus one of the following additions: 2 mM Mg–ATP; 0.5 M NaCl; 1 M NaCl; or 2 mM Mg–ATP plus 0.5 M NaCl. The samples were incubated for 30 min at 25°C and then centrifuged in a TLA 100 rotor for 30 min at 50,000 rpm at 25°C. Supernatants and pellets were resuspended in equivalent volumes of sample buffer and used for gel and immunoblot analysis.

SDS–polyacrylamide gel electrophoresis (SDS–PAGE) and electrophoretic transfer were performed according to routine protocols (Harlow and Lane, 1988). Immunoblots were blocked for at least 2 hr in 5% NFDM in TBST plus 0.1% NaN_3, rinsed, and incubated in primary antibody (0.1 μg/ml affinity-purified antibody diluted in 2% BSA in TBST plus 0.1% NaN_3), followed by horseradish peroxidase–conjugated secondary antibody (1:2500). Blots were rinsed and developed with enhanced chemiluminescence (Amersham).

Immunofluorescence

XL177 cells were grown on polylysine-coated glass coverslips to near confluency. Coverslips were rinsed in TBS, and then cells were fixed with 4% formaldehyde in BRB80 containing 5 mM EGTA for 20 min. Coverslips were processed essentially as described previously (Sawin et al., 1992b). All micrographs were taken on a Bio-Rad MRC-600 laser scanning confocal microscope. Series of optical sections through the cell were collected and projected onto a single image plane. Images were transferred to Adobe Photoshop, digitally processed, and printed on a Fujix Pictrography 3000 (Better Image Productions).

Extract-assembled spindles were prepared as described below. After methanol fixation, coverslips were washed in TBS–TX (TBS plus 0.1% Triton X-100), blocked, and stained with primary and secondary antibodies as above. DNA was visualized with 10 μg/ml Hoechst 33258, and the coverslips were mounted as above. Photomicrographs were taken on a Zeiss Photomicroscope III with Kodak Ektachrome Elite 200 film. Slides were printed and then scanned into a computer using a color scanner (UMAX Model PS-2400X). Images were collected in Adobe Photoshop and processed as above.

Spindle Assembly and Immunodepletion

CSF-arrested extracts were prepared essentially as described previously (Murray, 1991), except that the crushing spin was performed at 10,000 rpm for 15 min with full brake in an SW55 Ti rotor (Beckman). These extracts are technically meiosis II–arrested extracts, but are referred to as mitotic extracts or CSF extracts in this paper (see Sawin and Mitchison [1991] for a more detailed explanation). Mitotic spindle assembly was carried out as described previously (Sawin and Mitchison, 1991) using only freshly prepared extracts. The final concentration of sperm nuclei was 150 sperm per microliter. For immunodepletion experiments, we used CSF extract–assembled spindles because the process of immunodepletion often perturbed the extract sufficiently to inhibit cycled spindle assembly. For antibody addition experiments and for immunofluorescent staining of spindles, CSF extracts were cycled into interphase with the addition of Ca^{2+} and then back into mitosis with fresh CSF extract as described previously (Sawin and Mitchison, 1991; Shamu and Murray, 1992). Results from the two different types of extract preparations were indistinguishable.

For immunodepletions, Affi-Prep protein A beads (Bio-Rad) were washed three times in TBS–TX and then coated with affinity-purified antibodies to XKCM1 or with control rabbit IgG (Accurate Chemical and Scientific) for 1 hr at 4°C. The beads were washed one time with TBS–TX and three times with CSF–XB containing 10 μg/ml protease inhibitors (leupeptin, pepstatin A, and chymostatin). After the last wash, we removed as much liquid as possible so as not to dilute the extract. Freshly made CSF extract was added, and the mixture was gently rotated for 1 hr at 4°C. It was important to be very gentle in the immunodepletions or the extract would activate and become an interphase extract. After incubation of extract with beads, the beads were removed by centrifugation for 20 s in a microfuge at top speed. The supernatant was saved and used as the immunodepleted extract. The beads were washed three times in CSF–XB, one time in TBS–TX, and one time in TBS and then boiled in sample buffer before gel analysis. We used the ratio of 25 μl of beads:4 μg of antibody:200 μl of extract. For all immunodepletions, an equivalent volume of mock-depleted extract or XKCM1-depleted extract was analyzed by immunoblot to determine the extent of depletion. For antibody addition experiments, antibodies were added as one-tenth final volume diluted in sperm dilution buffer (5 mM K–HEPES [pH 7.7], 1 mM $MgCl_2$, 100 mM KCl, 150 mM sucrose).

For data quantitation, spindles were assembled as described above, and, at the indicated timepoint, 20 μl of the extract was removed and diluted into 2 ml of BRB80, 30% glycerol, 0.5% Triton X-100, 1 mM Mg–ATP. This was layered onto a cushion containing BRB80, 40% glycerol, 1 mM Mg–ATP and centrifuged onto coverslips at 6000 × g for 30 min at 16°C. Coverslips were postfixed in −20°C methanol, washed in TBS–TX, stained with Hoechst 33258,

and mounted as described above for immunofluorescence. Photographs were taken on a Zeiss Photomicroscope III. The results presented represent quantitated data from at least three individual experiments at three different timepoints with at least 250 nuclei counted for each datapoint. We observed qualitatively the same results with at least ten independent extracts.

Purification of XKCM1 from Extracts

XKCM1 was purified from high speed supernatants of Xenopus egg extracts by immunoaffinity chromatography. We prepared 25% ammonium sulfate supernatants as described elsewhere (Zheng et al., 1995) and froze them at −80°C until use. All steps were carried out at 4°C. The 25% ammonium sulfate supernatants were thawed, brought to 40% saturation with solid ammonium sulfate, rotated for 1 hr, and then pelleted at 27,000 × g for 15 min. The pellet was resuspended in MB1 (10 mM K–HEPES [pH 7.2], 2 mM $MgCl_2$, 100 mM KCl, 50 mM sucrose, 1 mM EGTA, 50 μM Mg–ATP, 0.1 mM DTT, 0.1 μg/ml protease inhibitors) and dialyzed against the same overnight. The dialyzed 25%–40% ammonium sulfate cut was clarified by centrifugation for 10 min at full speed in a microfuge before use. Affinity columns were prepared by washing Affi-Prep protein A beads three times in TBS–TX and then coating with affinity-purified XKCM1-CTP antibodies for 1 hr. We used a ratio of 25 μg of antibody:50 μl of beads:1 ml of extract. After antibody binding, the beads were washed one time in TBS–TX and four times in MB1. The washed beads were added to the clarified ammonium sulfate cuts and rotated for 2 hr. The mixture was poured into a column and then washed with 20 vol of MB1. To elute the XKCM1, we added 1 column volume of MB1 plus 250 μg/ml XKCM1 carboxy-terminal peptide to the resin, allowed it to flow in, and incubated it for 1 hr. The column was then eluted with 7 additional column volumes of MB1 plus 250 μg/ml XKCM1 carboxy-terminal peptide. Fractions were analyzed by SDS–PAGE. Fractions that contained pure XKCM1 were pooled, casein was added to 100 μg/ml as a carrier protein, and samples were concentrated 40-fold in Microcon-30 concentrators (Amicon). For the mock buffer control, we used MB1 plus 250 μg/ml XKCM1 carboxy-terminal peptide plus 100 μg/ml casein and concentrated it side by side with the purified XKCM1.

Reconstitution of Spindle Assembly with Purified XKCM1

Mitotic spindle assembly and immunodepletions were carried out as described above. For reconstitution of spindle assembly, extracts were immunodepleted and then one-tenth or one-fifth final volume of the pure XKCM1 or the mock buffer control was added to the extract. Spindles were allowed to assemble and then sedimented onto coverslips as described above. Images were recorded with an Olympus 60× 1.4 NA lens through a silicon-intensified target camera (COHU), which was controlled by Maxvision image processor (Datacube) driven by a 386 AT microcomputer. Images were recorded onto an optical memory disk recorder (Panasonic) and analyzed with Image-1 analysis software (Universal Imaging Corporation). We recorded area measurements for at least 50 nuclei in two independent experiments at two timepoints. Data were qualitatively observed with four independent preparations of XKCM1 protein on at least six different extracts.

Assaying Microtubule Dynamics

Mitotic extracts prepared as above were clarified as described (Hirano and Mitchison, 1993) and frozen in 50 μl aliquots. In the case of immunodepletions, extracts were immunodepleted as described above using a ratio of 75 μl of beads:12 μg of antibody:450 μl of extract before freezing in 50 μl aliquots. For assaying dynamics, an aliquot was thawed, diluted 2-fold with XBE2 (CSF–XB containing 2 mM $MgCl_2$) containing 1.5× energy mix (150 mM creatine phosphate, 20 mM ATP, 20 mM $MgCl_2$) and 37.5 μg/ml creatine kinase, and centrifuged for 5 min in a microfuge. For antibody addition experiments, affinity-purified anti-XKCM1 or control IgG was diluted to 0.5 mg/ml in sperm dilution buffer and added to the supernatant at 25 μg/ml on ice. Tetrahymena axonemes prepared as per Mitchison and Kirschner (1984) were washed by diluting 100-fold in XBE2 plus 0.1% Triton X-100, pelleted for 5 min in a microfuge, and resuspended to 10^7 per milliliter in XBE2. Axonemes were adhered to the coverslip for 3 min in a 5–8 μl flow cell prepared as described previously (Vale, 1991). Unadhered axonemes were washed out using 40 μl of XBE2, and 25 μl of clarified extract was flowed into the chamber. Assembly off axonemes was observed using VE-DIC microscopy for 20 min at 23°C–24°C, and the parameters describing microtubule dynamic instability were determined using home-written software according to the conventions of Walker et al. (1988). Under our experimental conditions, we were only able to calculate the rates of plus end microtubule dynamics. VE-DIC was performed using a Zeiss Axioplan microscope illuminated with a 50 W mercury lamp and equipped with a 1.4 NA condenser and a 63× 1.4 NA Planapochromatic objective. The image was projected using a 4× tube onto the target of a Hamamatsu Newvicon camera, and the image was averaged for four frames and contrast-enhanced using a Hamamatsu Argus 20 image processor. The enhanced, four frame–averaged image was stored on S-VHS videotape, which was used for analysis using a home-written program (W. Marshall and R. D. Vale, personal communication). Antibody addition and immunodepletion experiments were performed on separate extract preparations.

Acknowledgments

Correspondence should be addressed to C. E. W. We thank all the members of the Mitchison laboratory (past and present) for helpful comments, criticism, and discussion throughout the course of this work, especially Tatsuya Hirano for never-ending suggestions and Linda Wordeman and Ken Sawin, whose earlier work provided the inspiration for this project. We are grateful to YiXian Zheng for her generous donation of ammonium sulfate supernatants and to Wayne Forrester and Scott Ballantyne for molecular biology instruction. We are also thankful to Matt Welch and Karen Oegema for invaluable comments on the manuscript. This work was supported by a National Institutes of Health (NIH) grant (GM39565-07) and a grant from the Human Frontier Science Program (RG350/94) to T. J. M.; C. E. W. is an NIH postdoctoral fellow; A. D. is a Howard Hughes Medical Institute predoctoral fellow.

Received September 21, 1995; revised November 8, 1995.

References

Aizawa, H., Sekine, Y., Takemura, R., Zhang, Z., Nangaku, M., and Hirokawa, N. (1992). Kinesin family in murine central nervous system. J. Cell Biol. *119*, 1287–1296.

Bajer, A.S. (1982). Functional autonomy of monopolar spindle and evidence for oscillatory movement in mitosis. J. Cell Biol. *93*, 33–48.

Belmont, L.D., Hyman, A.A., Sawin, K.E., and Mitchison, T.J. (1990). Real-time visualization of cell cycle–dependent changes in microtubule dynamics in cytoplasmic extracts. Cell *62*, 579–589.

Chrétien, D., Fuller, S.D., and Karsenti, E. (1995). Structure of growing microtubule ends: two-dimensional sheets close into tubes at variable rates. J. Cell Biol. *129*, 1311–1328.

Desai, A., and Mitchison, T.J. (1995). A new role for motor proteins as couplers to depolymerizing microtubules. J. Cell Biol. *128*, 1–4.

Endow, S.A., Kang, S.J., Satterwhite, L.L., Rose, M.D., Skeen, V.P., and Salmon, E.D. (1994). Yeast Kar3 is a minus-end microtubule motor protein that destabilizes microtubules preferentially at the minus ends. EMBO J. *13*, 2708–2713.

Harlow, E., and Lane, D. (1988). Antibodies: A Laboratory Manual (Cold Spring Harbor, New York: Cold Spring Harbor Laboratory).

Hirano, T., and Mitchison, T.J. (1993). Topoisomerase II does not play a scaffolding role in the organization of mitotic chromosomes assembled in *Xenopus* egg extracts. J. Cell Biol. *120*, 601–612.

Hirose, K., Lockhart, A., Cross, R.A., and Amos, L.A. (1995). Nucleotide-dependent angular change in kinesin motor domain bound to tubulin. Nature *376*, 277–279.

Hoenger, A., Sablin, E.P., Vale, R.D., Fletterick, R.J., and Milligan, R.A. (1995). Three-dimensional structure of a tubulin-motor-protein complex. Nature *376*, 271–274.

Holy, T.E., and Leibler, S. (1994). Dynamic instability of microtubules

as an efficient way to search in space. Proc. Natl. Acad. Sci. USA *91*, 5682–5685.

Hyman, A.A., and Mitchison, T.J. (1990). Modulation of microtubule stability by kinetochores *in vitro*. J. Cell Biol. *110*, 1607–1616.

Hyman, A.A., and Mitchison, T.J. (1991). Two different microtubule-based motor activities with opposite polarities in kinetochores. Nature *351*, 206–211.

Inoué, S., and Salmon, E.D. (1995). Force generation by microtubule assembly/disassembly in mitosis and related movements. Mol. Biol. Cell, 1619–1640.

Kellogg, D.R., and Alberts, B.M. (1992). Purification of a multiprotein complex containing centrosomal proteins from the *Drosophila* embryo by chromatography with low-affinity polyclonal antibodies. Mol. Biol. Cell *3*, 1–11.

Kikkawa, M., Ishikawa, T., Wakabayashi, T., and Hirokawa, N. (1995). Three-dimensional structure of the kinesin head-microtubule complex. Nature *376*, 274–277.

Kirschner, M.W., and Mitchison, T.J. (1986). Beyond self assembly: from microtubules to morphogenesis. Cell *45*, 329–342.

Lohka, M.J., and Maller, J.L. (1985). Induction of nuclear envelope breakdown, chromosome condensation, and spindle formation in cell-free extracts. J. Cell Biol. *101*, 518–523.

Lombillo, V.A., Nislow, C., Yen, T.J., Gelfand, V.I., and McIntosh, J.R. (1995a). Antibodies to the kinesin motor domain and CENP-E inhibit microtubule depolymerization-dependent motion of chromosomes *in vitro*. J. Cell Biol. *128*, 107–115.

Lombillo, V.A., Stewart, R.J., and McIntosh, J.R. (1995b). Minus-end-directed motion of kinesin-coated microspheres driven by microtubule depolymerization. Nature *373*, 161–164.

Lupas, A., Van Dyke, M., and Stock, J. (1991). Predicting coiled coils from protein sequences. Science *252*, 1162–1164.

Mandelkow, E.M., Mandelkow, E., and Milligan, R.A. (1991). Microtubule dynamics and microtubule caps-a time-resolved cryo-electron microscopy study. J. Cell Biol. *114*, 977–991.

Mitchison, T.J., and Kirschner, M.W. (1984). Dynamic instability of microtubule growth. Nature *312*, 237–242.

Murray, A.W. (1991). Cell cycle extracts. In Methods in Cell Biology, B.K. Kay and H.B. Peng, eds. (San Diego, California: Academic Press), pp. 581–605.

Pfarr, C.M., Coue, M., Grisson, P.M., Hays, T.S., Porter, M.E., and McIntosh, J.R. (1990). Cytoplasmic dynein is localized to kinetochores during mitosis. Nature *345*, 263–265.

Rieder, C.L., and Salmon, E.D. (1994). Motile kinetochores and polar ejection forces dictate chromosome position on the vertebrate mitotic spindle. J. Cell Biol. *124*, 223–233.

Salmon, E.D., Leslie, R.J., Karow, W.M., McIntosh, J.R., and Saxton, R.J. (1984). Spindle microtubule dynamics in sea urchin embryos: analysis using fluorescence-labeled tubulin and measurements of fluorescence redistribution after laser photobleaching. J. Cell Biol. *99*, 2165–2174.

Sambrook, J., Fritsch, E., and Maniatis, T. (1989). Molecular Cloning: A Laboratory Manual (Cold Spring Harbor, New York: Cold Spring Harbor Laboratory Press).

Sawin, K.E., and Mitchison, T.J. (1991). Mitotic spindle assembly by two different pathways *in vitro*. J. Cell Biol. *112*, 925–940.

Sawin, K.E., LeGuellec, K., Philippe, M., and Mitchison, T.J. (1992a). Mitotic spindle organization by a plus-end directed microtubule motor. Nature *359*, 540–543.

Sawin, K.E., Mitchison, T.J., and Wordeman, L.G. (1992b). Evidence for kinesin-like proteins in the mitotic apparatus using peptide antibodies. J. Cell Sci. *102*, 303–313.

Saxton, W.M., Stemple, D.L., Leslie, R.J., Salmon, E.D., Zavortink, M., and McIntosh, J.R. (1984). Tubulin dynamics in cultured mammalian cells. J. Cell Biol. *99*, 2175–2186.

Shamu, C.E., and Murray, A.W. (1992). Sister chromatid separation in frog egg extracts requires DNA topoisomerase II activity during anaphase. J. Cell Biol. *117*, 921–934.

Skibbens, R., Skeen, V.P., and Salmon, E.D. (1993). Directional instability of kinetochore motility during chromosome congression and segregation in mitotic newt lung cells: a push-pull mechanism. J. Cell Biol. *122*, 859–875.

Smith, D.B., Rubira, M.R., Simpson, R.J., Davern, K.M., Tui, W.U., Board, P.G., and Mitchell, G.F. (1988). Expression of an enzymatically-active parasite molecule in *Escherichia coli*: *Schistosoma japonicum* glutathione S-transferase. Mol. Biochem. Parasitol. *27*, 249–256.

Steuer, E.R., Wordeman, L., Schroer, T.A., and Sheetz, M.P. (1990). Localization of cytoplasmic dynein to mitotic spindles and kinetochores. Nature *345*, 266–268.

Vale, R.D. (1991). Severing of stable microtubules by a mitotically activated protein in Xenopus egg extracts. Cell *64*, 827–839.

Verde, F., Labbe, J.-c., Doree, M., and Karsenti, E. (1990). Regulation of microtubule dynamics by cdc2 protein kinase in cell-free extracts of *Xenopus* eggs. Nature *343*, 233–238.

Verde, F., Dogterom, M., Stelzer, E., Karsenti, E., and Leibler, S. (1992). Control of microtubule dynamics and length by cyclin A- and cyclin B-dependent kinases in *Xenopus* egg extracts. J. Cell Biol. *118*, 1097–1108.

Vernos, I., Raats, J., Hirano, T., Heasman, J., Karsenti, E., and Wylie, C. (1995). Xklp1, a chromosomal Xenopus kinesin-like protein essential for spindle organization and chromosome positioning. Cell *81*, 117–127.

Walker, R.A., O'Brien, E.T., Pryer, N.K., Sobeiro, M.F., Voter, W.A., Erickson, H.P., and Salmon, E.D. (1988). Dynamic instability of individual microtubules analysed by video light microscopy: rate constants and transition frequencies. J. Cell Biol. *107*, 1437–1448.

Wordeman, L., and Mitchison, T. (1995). Identification and partial characterization of mitotic centromere-associated kinesin, a kinesin-related protein that associates with centromeres during mitosis. J. Cell Biol. *128*, 95–105.

Yen, T.J., Compton, D.A., Wise, D., Zinkowski, R.P., Brinkley, B.R., Earnshaw, W.C., and Cleveland, D.W. (1991). CENP-E, a novel human centromere-associated protein required for progression from metaphase to anaphase. EMBO J. *10*, 1245–1254.

Zheng, Y., Wong, M., Alberts, B., and Mitchison, T. (1995). Nucleation of microtubule assembly by a γ-tubulin containing ring complex. Nature *378*, 578–583.

GenBank Accession Numbers

The sequence of XKCM1 is available under accession number U36485; the sequence for XKIF2 described in this report is available under accession number U36486.

Note Added in Proof

The authors inadvertently left out the citation for the work describing mouse KIF2 localization and motility. The correct reference is: Noda, Y., Sato-Yoshitake, R., Kondo, S., Nangaku, M., and Hirokawa, N. KIF2 is a new microtubule-based anterograde motor that transports membranous organelles distinct from those carried by kinesin heavy chain or KIF3A/B. J. Cell Biol. *129*, 157–167, 1995.